ACS OMEGA

http://pubs.acs.org/journal/acsodf

Article

# Impact of Zero-Valent Iron Nanoparticles on *Fremyella diplosiphon* Transesterified Lipids and Fatty Acid Methyl Esters

Somayeh Gharaie Fathabad, Behnam Tabatabai, Dy'mon Walker, Huan Chen, Jie Lu, Kadir Aslan, Jamal Uddin, William Ghann, and Viji Sitther*

Cite This: https://dx.doi.org/10.1021/acsomega.0c00566

Read Online

ACCESS | Metrics & More | Article Recommendations | Supporting Information

**ABSTRACT:** Efforts to enhance the transformative potential of biofuels is an important step to achieving an environment-friendly and sustainable energy source. *Fremyella diplosiphon* is an ideal third-generation biofuel agent due to its ability to produce lipids and desirable essential fatty acids. In this study, the impact of Nanofer 25s nanoscale zero-valent iron nanoparticles (nZVIs) on total lipid content and fatty acid composition of *F. diplosiphon* strains SF33 and B481 was investigated. We observed significant increases ($P < 0.05$) in the growth of *F. diplosiphon* treated with 0.2−1.6 mg $L^{-1}$ Nanofer 25s, indicating that trace concentrations of nZVIs were not toxic to the organism. Chlorophyll *a*, carotenoids, and phycobiliprotein levels were not altered in *F. diplosiphon* treated with nZVIs ranging from 0.4 to 1.6 mg $L^{-1}$, confirming that these concentrations did not negatively impact photosynthetic efficacy. In addition, Nanofer 25s ranging from 0.2 to 1.6 mg $L^{-1}$ had an optimal impact on SF33 and B481 total lipid content. We identified significant increases in unsaturated fatty acid methyl esters (FAMEs) from *F. diplosiphon* Nanofer 25s-treated transesterified lipids. Theoretical chemical and physical biofuel properties revealed a product with elevated cetane number and oxidative stability for both strains. Scanning electron microscopy and energy-dispersive X-ray spectroscopy validated the localization of nZVIs. Our findings indicate that Nanofer 25s nZVIs significantly enhance *F. diplosiphon* total lipid content and essential FAMEs, thus offering a promising approach to augment the potential of the cyanobacterium as a large-scale biofuel agent.

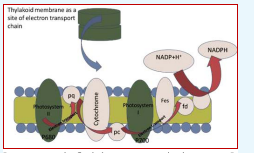


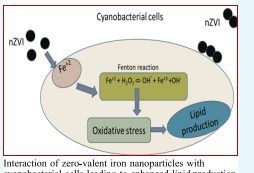


## INTRODUCTION

The ever-increasing energy demand and hazardous effects of petroleum-based fossil fuels have driven great necessity to accelerate the development of environmentally friendly nonpolluting alternatives. As photosynthetic microorganisms, cyanobacteria offer an efficient biofuel platform due to their fast growth rate, high lipid production capacity, and ability to thrive in varying nutrient stress.[1−3] To make biofuels more competitive with fossil fuels, innovative approaches to enhance lipids, which are the raw material for biodiesel production, have been pursued. In recent years, metallic nanoparticles have gained significant eminence in biodiesel production due to their higher surface area/volume ratio characteristics, reactivity, and light-scattering properties due to plasmon resonance.[4,5] These nanomaterials are known to enhance biohydrogen, biogas, and bioethanol production, thus increasing energy-conversion efficiency.[6]

Of the various types of nanomaterials, nanoscale zero-valent iron nanoparticles (nZVIs) have been widely used to improve the activity of microbial communities. Enhanced cell growth and metabolic activity of photosynthetic microorganisms have been reported using these nZVIs.[7,8] In addition to improving methane in biogas production by 30.4%, these nZVIs resulted in a 98% reduction in hydrogen sulfide concentration.[9] With the core−shell structure of zero-valent iron acting as an electron donor to compounds, the oxide shell consists of iron oxides and hydroxides (FeOOH), providing active sites for complex chemical reactions to occur.[10]

Of the various species of photosynthetic microbes, *Fremyella diplosiphon* is a model cyanobacterium that exhibits an impressive response to stress factors.[11,12] With abundant C16:1 and C18:1 fatty acids (FAs) and high-value fatty acid methyl esters (FAMEs) in its transesterified lipids, this species is an ideal candidate for high-quality biofuel production.[13] While studies have focused on the interactions between light and iron acclimation resulting in enhanced *F. diplosiphon* photosynthetic efficacy,[12,14] to our knowledge the effect of nZVIs on total lipid yield and fatty acid (FA) composition of this organism has not been explored. Development of novel methods to enhance cyanobacterial biomass and overproduce lipids would lead to a sustainable low-cost system to produce biofuels. In the present study, we identified nontoxic concentrations of nZVIs that induce optimal *F. diplosiphon* growth and photosynthetic pigmentation. Furthermore, we evaluated the impact of these nZVIs on *F. diplosiphon* total

Received: February 7, 2020
Accepted: May 6, 2020

lipid content and FAMEs. Theoretical chemical and physical biodiesel properties were calculated to evaluate the potential of nZVIs for *F. diplosiphon* biofuel production.

## RESULTS

**Growth and Photosynthetic Pigments of *F. diplosiphon* in Varying nZVI Concentrations.** To investigate the effect of nanoparticle-mediated iron stress, *F. diplosiphon* strains were grown in media containing Nanofer 25s nZVIs ranging from 0.05 to 3.2 mg $L^{-1}$ and growth was compared to the control. We observed significant increases ($P < 0.05$) in the growth of B481 and SF33 strains exposed to 0.2, 0.4, 0.8, and 1.6 mg $L^{-1}$ Nanofer 25s. However, cultures exposed to 0.05, 0.1, and 3.2 mg $L^{-1}$ Nanofer 25s did not exhibit significant differences ($P < 0.05$) in growth (Figure 1). In addition, we did

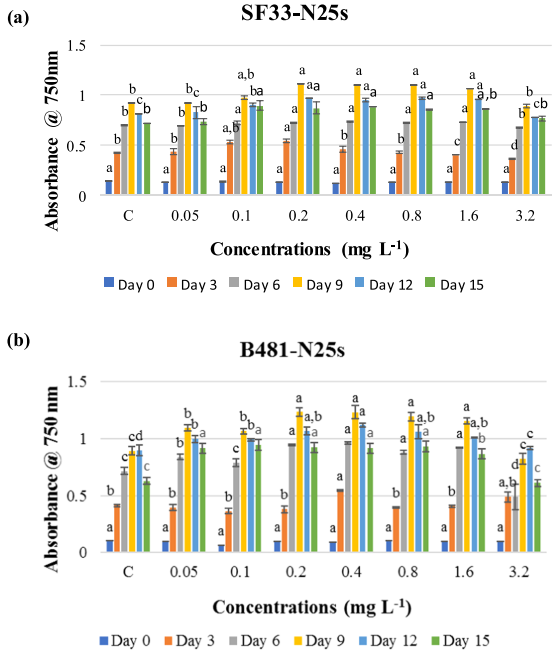


**Figure 1.** Growth of *F. diplosiphon* strains (a) SF33 and (b) B481 in BG11/HEPES medium with 0.05, 0.1, 0.2, 0.4, 0.8, 1.6, and 3.2 mg $L^{-1}$ Nanofer 25s over a period 15 days. Average optical density at 750 nm (±standard error) for three biological replicates is shown for each time point. Different letters above the final time point indicate significance among treatment means ($P < 0.05$).

not observe significant differences in photosynthetic efficacy of both *F. diplosiphon* strains at these *t* concentrations. (Figure S1). No significant differences ($P > 0.05$) in chlorophyll *a* (chl*a*) (Figure S2a), carotenoid (Figure S2b), and phycobiliprotein levels including phycocyanin (Figure S3a), allophycocyanin (Figure S3b), and phycoerythrin (Figure S3c) in *F. diplosiphon* exposed to Nanofer 25s ranging from 0.4 to 1.6 mg $L^{-1}$ were observed.

**Evaluation of Total Lipid Content in *F. diplosiphon* Nanofer 25s-Treated Cells.** Since both strains cultivated with Nanofer 25s ranging from 0.2 to 1.6 mg $L^{-1}$ revealed a significant enhancement in growth, we compared total lipid content of nZVI-treated cultures to the control. Gravimetric analysis revealed significant increases ($P < 0.05$) in total lipid content of strain B481 when exposed to 0.4, 0.8, and 1.6 mg $L^{-1}$ Nanofer 25s while significant increases ($P < 0.05$) in SF33 total lipid yield were observed in cultures grown in 0.2−1.6 mg $L^{-1}$ Nanofer 25s (Figure 2). No significant differences ($P > 0.05$) were detected in B481 total lipid content when exposed

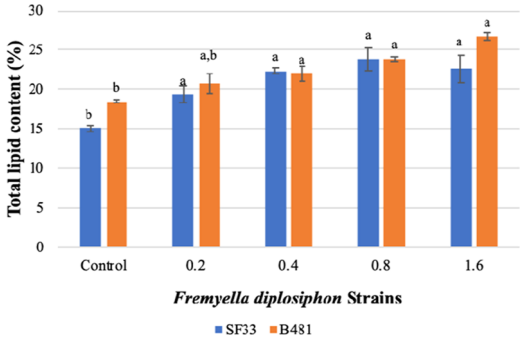


**Figure 2.** Comparison of total lipid content in *F. diplosiphon* strains SF33 and B481 control and cultures grown with 0.2, 0.4, 0.8, and 1.6 mg $L^{-1}$ Nanofer 25s. Average percent lipid content (±standard error) of three biological replicates for each strain is shown. Different letters above bars indicate significance among treatment means ($P < 0.05$).

to 0.2 mg $L^{-1}$ Nanofer 25s. Furthermore, we detected 22.57, 7.04, 0.02, and 18.29% increases in lipid yield in *F. diplosiphon* B481 exposed to Nanofer 25s ranging from 0.2 to 1.6 mg $L^{-1}$ compared to SF33 exposed to the identical nZVI concentrations.

**Characterization of FAMEs in Nanofer 25s-Treated Cells by Gas Chromatography−Mass Spectrometry (GC−MS) and GC × GC-Time-of-Flight Mass Spectrometry (TOFMS).** We detected saturated and unsaturated FAMEs in *F. diplosiphon* nanotreated cultures and the untreated control (Table 1). Methyl palmitate, which is the

**Table 1. Breakdown of Saturated and Unsaturated Fatty Acid Methyl Ester (FAME) Proportions in *F. diplosiphon* SF33 and B481 Control and Cultures Treated with 0.2, 0.4, 0.8, and 1.6 mg $L^{-1}$ Nanofer 25s**

| | FAME type (%) | | ratio of FAME |
|---|---|---|---|
| strains | saturated | unsaturated | saturated/ unsaturated |
| SF33 control | 88.64 | 11.44 | 7.75 |
| SF33 + 0.2 mg $L^{-1}$ N25s | 65.78 | 34.22 | 1.92 |
| SF33 + 0.4 mg $L^{-1}$ N25s | 62.67 | 37.33 | 1.68 |
| SF33 + 0.8 mg $L^{-1}$ N25s | 71.66 | 28.34 | 2.53 |
| SF33 + 1.6 mg $L^{-1}$ N25s | 50.50 | 49.50 | 1.02 |
| B481 control | 77.27 | 22.74 | 3.40 |
| B481 + 0.2 mg $L^{-1}$ N25s | 69.11 | 30.95 | 2.23 |
| B481 + 0.4 mg $L^{-1}$ N25s | 62.00 | 36.97 | 1.68 |
| B481 + 0.8 mg $L^{-1}$ N25s | 58.35 | 41.72 | 1.40 |
| B481 + 1.6 mg $L^{-1}$ N25s | 63.51 | 36.50 | 1.74 |

methyl ester of hexadecanoic acid (C16:0), was detected as the dominant FAME in the nanotreated and control cultures. This component accounted for 82.55, 59.67, 56.64, 69.69, and 49.05% of total FAMEs produced from SF33 treated with Nanofer 25s ranging from 0 to 1.6 mg $L^{-1}$ total lipids and 66.00, 61.43, 57.87, 55.42, and 60.95% from B481 treated at the same concentrations (Table 2). Additional FAME components such as methyl tetradecanoate (C14:1), methyl hexadecanoate (C16:1), methyl octadecanoate (C18:0), methyl octadecenoate (C18:1), and methyl octadecadienoate (C18:2) were detected in all *F. diplosiphon* cultures (Figure 3


https://dx.doi.org/10.1021/acsomega.0c00566
ACS Omega XXXX, XXX, XXX−XXX

Table 2. Fatty Acid Methyl Ester (FAME) Composition in *F. diplosiphon* SF33 and B481 Control and 0.2, 0.4, 0.8, and 1.6 mg $L^{-1}$ Nanofer 25s-Treated Cultures

| FAME | control | 0.2 mg $L^{-1}$ | 0.4 mg $L^{-1}$ | 0.8 mg $L^{-1}$ | 1.6 mg $L^{-1}$ |
|---|---|---|---|---|---|
| strain SF33 | | | | | |
| methyl myristate (C14:1) | 2.19 ± 0.86 | 15.07 ± 3.62 | 7.82 ± 3.40 | 4.98 ± 2.42 | 14.36 ± 9.78 |
| methyl palmitate (C16:0) | 82.55 ± 6.87 | 59.67 ± 9.75 | 56.64 ± 13.85 | 69.69 ± 2.57 | 49.05 ± 14.61 |
| methyl hexadecanoate (C16:1) | 3.33 ± 1.28 | 9.16 ± 1.79 | 14.02 ± 3.09 | 7.39 ± 2.99 | 24.27 ± 4.75 |
| methyl octadecanoate (C18:0) | 6.09 ± 3.46 | 6.11 ± 1.98 | 6.03 ± 2.40 | 1.97 ± 1.42 | 1.45 ± 1.20 |
| methyl octadecenoate (C18:1) | 3.44 ± 2.82 | 6.19 ± 1.41 | 8.48 ± 3.82 | 8.35 ± 4.59 | 6.81 ± 4.58 |
| methyl octadecadienoate (C18:2) | 2.49 ± 2 | 3.80 ± 1.74 | 7.01 ± 3.49 | 7.63 ± 1.97 | 4.06 ± 3.30 |
| strain B481 | | | | | |
| methyl myristate (C14:1) | 8.73 ± 4.67 | 12.20 ± 0.58 | 4.92 ± 2.31 | 10.17 ± 4.64 | 3.10 ± 1.55 |
| methyl palmitate (C16:0) | 66.00 ± 5.25 | 61.43 ± 9.65 | 57.87 ± 4.31 | 55.24 ± 9.49 | 60.95 ± 1.11 |
| methyl hexadecanoate (C16:1) | 9.66 ± 3.99 | 8.45 ± 2.82 | 22.01 ± 1.38 | 15.00 ± 8.66 | 10.09 ± 6.55 |
| methyl octadecanoate (C18:0) | 11.27 ± 5.87 | 7.68 ± 4.76 | 4.13 ± 0.95 | 3.10 ± 1.08 | 2.56 ± 0.11 |
| methyl octadecenoate (C18:1) | 1.49 ± 0.69 | 5.32 ± 0.26 | 5.04 ± 0.56 | 10.09 ± 1.88 | 15.02 ± 13.46 |
| methyl octadecadienoate (C18:2) | 2.86 ± 0.66 | 4.98 ± 1.75 | 5.01 ± 2.07 | 6.46 ± 1.96 | 8.29 ± 4.14 |

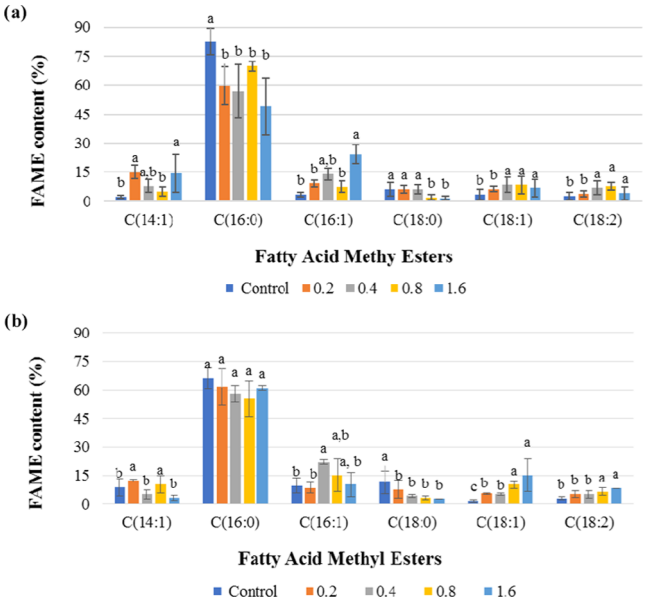


**Figure 3.** Comparison of fatty acid methyl ester (FAME) composition of *F. diplosiphon* strains (a) SF33 and (b) B481 total lipids subjected to direct transesterification in untreated control and 0.2, 0.4, 0.8, and 1.6 mg $L^{-1}$ Nanofer 25s. Average percent FAME content (±standard error) for three biological replicates of each strain is shown. Different letters above bars indicate significance among treatment means ($P < 0.05$).

and Table 2). While a significant increase ($P < 0.05$) in methyl octadecenoate (C18:1) and methyl octadecadienoate (C18:2) levels was observed in SF33 transesterified lipids exposed to 0.4, 0.8, and 1.6 mg $L^{-1}$ Nanofer 25s (Figure 3a), no significant differences ($P > 0.05$) were observed in cultures treated with 0.2 mg $L^{-1}$ Nanofer 25s (Figure 3b). In addition, a significant increase ($P < 0.05$) in methyl octadecenoate (C18:1) and methyl octadecadienoate (C18:2) levels from B481 transesterified lipids treated at 0.8 and 1.6 mg $L^{-1}$ Nanofer 25s was observed. No significant differences were detected in SF33 (Figure 3a) and B481 transesterified lipids treated with 0.2 and 0.4 mg $L^{-1}$ Nanofer 25s (Figure 3b).

In addition to conventional GC−MS, high-resolution GC × GC−TOFMS was used to further separate polar and aromatic compounds. GC × GC−TOFMS analysis revealed the presence of FAMEs with numbers of carbon (C) from 12 to 18, double bonds from 0 to 4, and alkanes from $C_{11}$ to $C_{34}$. Sample chromatograms of SF33 control (Figure 4a) and cells treated with nZVIs at 1.6 mg $L^{-1}$ (Figure 4b) are shown. FAME abundance in SF33 and B481 strains treated with 0.8 and 1.6 mg $L^{-1}$ Nanofer 25s was significantly higher ($P < 0.05$) than the control. FAME components such as C18:3 and C18:4, which were not detected in conventional GC−MS, were identified by GC × GC−TOFMS. We observed that methyl octadecatrienoate (C18:3) in SF33 strain grown with 0.8 and 1.6 mg $L^{-1}$ Nanofer 25s (16 and 13.41% transesterified lipids) was significantly higher ($P < 0.05$) (Figure 5a). Octadecatrienoic acid (C18:3) in B481 strain treated with 0.8 and 1.6 mg $L^{-1}$ nZVIs was also significantly higher ($P < 0.05$), while methyl stearidonate (C18:4) was significantly lower (20.83 and 16% transesterified lipids). In addition, B481 strain treated with 0.8 and 1.6 mg $L^{-1}$ Nanofer 25s exhibited significant increases ($P < 0.05$) in methyl stearidonate (C18:4) (62.73 and 31.95% transesterified lipids) compared to the control (Figure 5b). Calculation of chemical and physical biofuel properties revealed products with a high cetane number (62.6−68.81 for SF33 and 63.0−67.74 for B481) and oxidative stability (49.38−18.04 h for SF33 and 43.82−16.81 h for B481) (Tables 3 and 4).

**Validation of nZVIs in *F. diplosiphon* Using Field-Emission Scanning Electron Microscopy (FESEM) and Energy-Dispersive Spectrometry (EDS).** FESEM equipped with EDS allowed visualization and distribution of nZVIs in *F. diplosiphon* (Figure 6). The small-sized nanoparticles with a higher surface area resulted in aggregation. We used elemental analysis by atomic percentages as a semiquantitative method to correlate the nZVI concentrations in the control and treatments. EDS measurement performed in one representative region where nZVIs aggregated is shown in Figure 6. No iron peak was observed in the spectrum of the control culture (Figure 6b). The percentage of iron in the EDS spectrum for *F. diplosiphon* grown with 3.2 mg $L^{-1}$ Nanofer 25s was 3.53%, while that with 0.8 mg $L^{-1}$ was 0.02% (Figure 6c,d). We observed other elements including oxygen, carbon, sodium, sulfur, chlorine, phosphorus, and silicon as well.

## DISCUSSION

Biofuels have clear advantages over fossil fuels as they offer a sustainable, efficient, and environmentally conscious energy source; however, there is an imminent need to maximize their


https://dx.doi.org/10.1021/acsomega.0c00566
ACS Omega XXXX, XXX, XXX−XXX

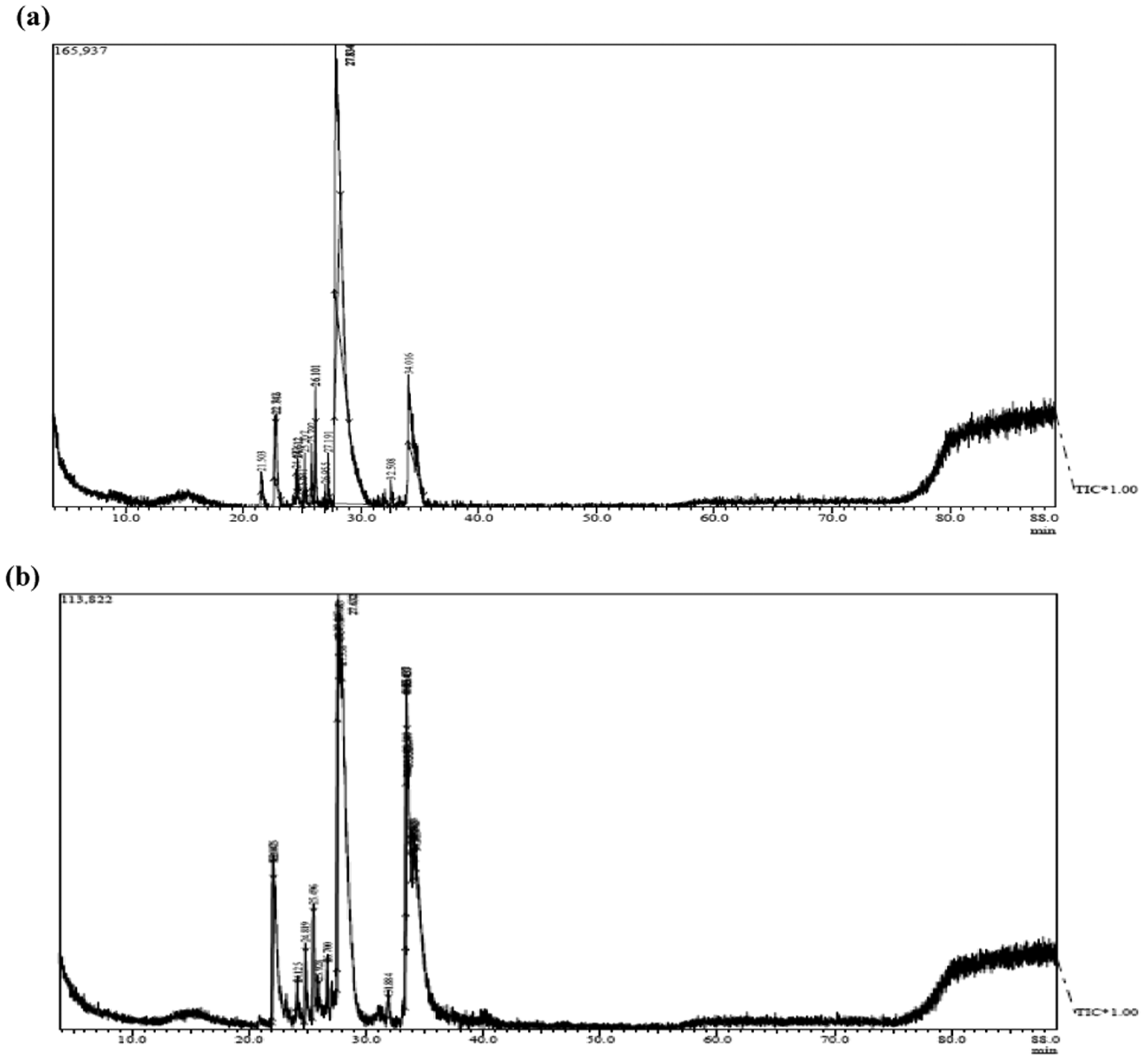


**Figure 4.** Representative one-dimensional (1-D) gas chromatogram of *F. diplosiphon* strain SF33 (a) control and (b) nanotreated cell (1.6 mg $L^{-1}$ Nanofer 25s) total lipids subjected to direct transesterification.

yields for these fuels to be competitive in the energy market. Concentrated carbon dioxide released from fossil fuel and industrial emissions is efficiently captured by algae and cyanobacteria and used in the process of photosynthesis. A comparison of carbon dioxide from petroleum and algae-based fuels indicates significantly lower emissions from biodiesel, with a 68% reduction in total emissions in cultivation ponds.[15] By creating additional physiological stress such as nutrient starvation or salinity, it is possible to increase lipid accumulation leading to scale-up in biodiesel production.[16] In this study, we tested the metal-induced stress of nZVIs on the biofuel-producing potential of *F. diplosiphon*.

While we observed significant increases in growth of SF33 and B481 strains treated with Nanofer 25s nZVIs ranging from 0.2 to 1.6 mg $L^{-1}$ (Figure 1), Nanofer 25 did not improve cell growth. It is possible that the extra coating of tetraethyl orthotalebite could have increased nZVI Nanofer 25s reactivity and stability, resulting in enhanced growth of the strains.[17] As reported by Pádrová et al.,[8] a key advantage of using Nanofer 25s nZVIs is their protection from rapid oxidation in the air due to their specific core, which contain zero-valent iron covered by an organic/inorganic protective shell resulting in a strong oxidation−reduction potential. Coated iron nanoparticles have been previously reported to stimulate *Escherichia coli* growth in different trichloroethylene-contaminated sites as well.[18]

Since high concentrations of nanoparticles could affect cyanobacterial photosynthetic pathways, we investigated pigment accumulation in Nanofer25s-treated cells. No significant differences in pigment accumulation or phycobiliprotein were observed in cells treated with trace concentrations of Nanofer 25s ranging from 0.05 to 3.2 mg $L^{-1}$, indicating that these pathways were not affected. These results are in accordance to a previous report, where no significant differences ($P > 0.05$) in carotenoid levels of the microalgae *Arthrospira platensis* treated with 10 mg $L^{-1}$ $Fe^{+2}$ were observed.[19] It is also possible that iron nanoparticles can enhance pigment accumulation when exposed to nanoparticles. A 30% increase in chl*a* content of


https://dx.doi.org/10.1021/acsomega.0c00566
ACS Omega XXXX, XXX, XXX−XXX

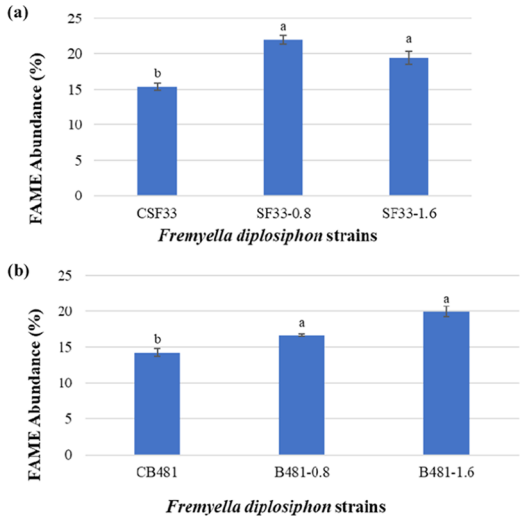


**Figure 5.** Fatty acid methyl ester (FAME) abundance in transesterified extractable lipids of *F. diplosiphon* (a) SF33 control (CSF33) and 0.8 and 1.6 mg $L^{-1}$ Nanofer 25s-treated cells (SF33, 0.8 and SF33, 1.6) and (b) B481 control (CB481) and 0.8 and 1.6 mg $L^{-1}$ Nanofer 25s-treated cells (B481, 0.8 and B481, 1.6) determined by GC × GC−TOFMS. Average percent FAME content (± coefficient of variation) of each strain for three biological replicates is shown. Different letters above bars indicate significance among treatment means ($P < 0.05$).

*Chlorella vulgaris* was reported when exposed to 100 mg $L^{-1}$ $Fe_2O_3$ nanoparticles.[20] However, unlike microalgae, our findings indicate that *F. diplosiphon* require trace amounts of nZVIs for efficient growth and pigment accumulation.

While the application of nZVIs in green technologies can be toxic to microorganisms due to damage caused by reactive oxygen species (ROS) activity, nonlethal levels of oxidative stress have been known to increase lipid yield in cyanobacterial and microalgal cells.[21] As Nanofer 25s-catalyzed nicotinamide adenine dinucleotide phosphate (NADP) (H)-dependent reactions are a primary source of ROS,[8] it is possible that oxidative stress induced by these nZVIs could have augmented lipid production.[21] Our findings revealed a 28−58% increase in total lipid content of strain SF33 and 19−44% in B481 treated with 0.2−1.6 mg $L^{-1}$ Nanofer 25s (Figure 2), indicating that iron stress enhanced *F. diplosiphon* lipid production. The results of our study are in accordance to a previous report where a total lipid yield of 26.2−35% was observed in the algae, *Trachydiscus minutus*, when cultivated with 5.1 mg $L^{-1}$ nZVIs.[8] Titanium oxide nanoparticles at 0.1 g $L^{-1}$ have also been reported to induce the generation of ROS, resulting in maximum lipid content in *C. vulgaris*.[22]

Quantification of total lipid content provides valuable information on the organism's lipid capacity; however, it is not exclusively determinative of the biofuel potential since this includes not only FAs but also all cellular lipids. Thus, it is vital to evaluate the FAME composition of *F. diplosiphon* transesterified lipids and examine the physico-chemical properties to gain a more comprehensive understanding of its biofuel quality. Higher methyl octadecadienoate (C18:1) and methyl octadecadienoate (C18:2) abundance in both strains (Figure 3) as observed in our study indicate the suitability of nZVIs to enhance unsaturated FAMEs, the primary components of biofuel. The suitability of a strain as a biofuel agent is also determined by the properties of fatty esters such as carbon chain length and degree of unsaturation.[23,24] Under oxidative stress, free radicals could alter various physiological functions. It is known that double bonds in unsaturated FAs possess a radical scavenging potential, which is known to contribute to cell protection against increased ROS activity.[25] The high accumulation of unsaturated FAs in nZVI-treated *F. diplosiphon* cells as observed in our study could be a cellular response to oxidative stress. We also observed an increase in essential unsaturated FAs such as oleic and linoleic acids in nZVI-treated cultures, suggesting their impact on *F. diplosiphon* lipid yield. This is not surprising since several major physiological processes such as cyanobacterial respiration, photosynthesis, and cell proliferation are influenced by iron.[12,26] In cyanobacteria, photosynthetic complexes require about 22−23 Fe atoms for photosystem I and II to act efficiently. Iron serves as a terminal electron acceptor, providing electrons to convert nicotinamide adenine dinucleotide phosphate (NADP) to reduced NADP (NADPH), which is a primary source of ROS in photosystem I in the cyanobacterial thylakoid membrane.[27] It is possible that nZVIs could have augmented lipid production by providing an ideal source of iron.

GC × GC−TOFMS offers a more efficient resolution, extra sensitivity, and accuracy of lipid analysis by the modulation process. With this advanced analytical technique, we found a significant increase in FAME abundance of *F. diplosiphon* when

**Table 3. Theoretical Biodiesel Properties of *F. diplosiphon* Transesterified Lipids in the SF33 Control and Cultures Treated with 0.2, 0.4, 0.8, and 1.6 mg $L^{-1}$ Nanofer 25s**

| biodiesel properties | control | 0.2 mg $L^{-1}$ | 0.4 mg $L^{-1}$ | 0.8 mg $L^{-1}$ | 1.6 mg $L^{-1}$ |
|---|---|---|---|---|---|
| saponification value (mg KOH $g^{-1}$ fat) | 217.314 | 219.319 | 216.413 | 216.344 | 220.219 |
| iodine value (g $I_2$/100 g) | 11.564 | 21.595 | 34.321 | 28.708 | 37.709 |
| cetane number | 68.814 | 66.327 | 63.798 | 65.069 | 62.6 |
| long chain saturated factor | 10.181 | 9.022 | 8.679 | 7.954 | 5.63 |
| cold filter plugging point (°C) | 15.509 | 11.867 | 10.79 | 8.512 | 1.211 |
| cloud point (°C) | 39.434 | 26.394 | 24.801 | 31.665 | 20.808 |
| pour point (°C) | 35.987 | 21.832 | 20.101 | 27.553 | 15.768 |
| allylic position equivalent | 8.66 | 13.79 | 22.5 | 23.61 | 14.93 |
| bis-allylic position equivalent | 2.52 | 3.8 | 7.01 | 7.63 | 4.06 |
| oxidation stability (h) | 49.388 | 33.625 | 19.414 | 18.047 | 31.637 |
| higher heating value (mJ $kg^{-1}$) | 39.244 | 39.116 | 39.18 | 39.199 | 39.053 |
| kinematic viscosity ($mm^2$ $s^{-1}$) | 3.808 | 3.651 | 3.681 | 3.718 | 3.508 |
| density (g $cm^{-3}$) | 0.868 | 0.868 | 0.87 | 0.869 | 0.87 |


https://dx.doi.org/10.1021/acsomega.0c00566
ACS Omega XXXX, XXX, XXX−XXX

Table 4. Theoretical Biodiesel Properties of *F. diplosiphon* Transesterified Lipids in B481 Control and Cultures Treated with 0.2, 0.4, 0.8, and 1.6 mg $L^{-1}$ Nanofer 25s

| biodiesel properties | control | 0.2 mg $L^{-1}$ | 0.4 mg $L^{-1}$ | 0.8 mg $L^{-1}$ | 1.6 mg $L^{-1}$ |
|---|---|---|---|---|---|
| saponification value (mg KOH/g fat) | 217.659 | 218.284 | 215.022 | 217.602 | 214.292 |
| iodine value (g $I_2$/100 g) | 16.165 | 22.241 | 35.582 | 35.751 | 38.597 |
| cetane number | 67.739 | 66.3 | 63.678 | 63.339 | 63.086 |
| long chain saturated factor | 12.235 | 9.983 | 7.852 | 7.074 | 7.375 |
| cold filter plugging point (°C) | 21.962 | 14.887 | 8.192 | 5.747 | 6.693 |
| cloud point (°C) | 29.724 | 27.32 | 25.448 | 24.064 | 27.068 |
| pour point (°C) | 25.446 | 22.837 | 20.804 | 19.302 | 22.562 |
| allylic position equivalent | 7.21 | 15.28 | 15.06 | 23.01 | 31.6 |
| bis-allylic position equivalent | 2.86 | 4.98 | 5.01 | 6.46 | 8.29 |
| oxidation stability (h) | 43.825 | 26.271 | 26.129 | 20.846 | 16.816 |
| higher heating value (mJ/kg) | 39.186 | 39.175 | 38.753 | 39.167 | 39.242 |
| kinematic viscosity ($mm^2$ $s^{-1}$) | 3.759 | 3.696 | 3.588 | 3.631 | 3.737 |
| density (g $cm^{-3}$) | 0.867 | 0.869 | 0.861 | 0.87 | 0.87 |

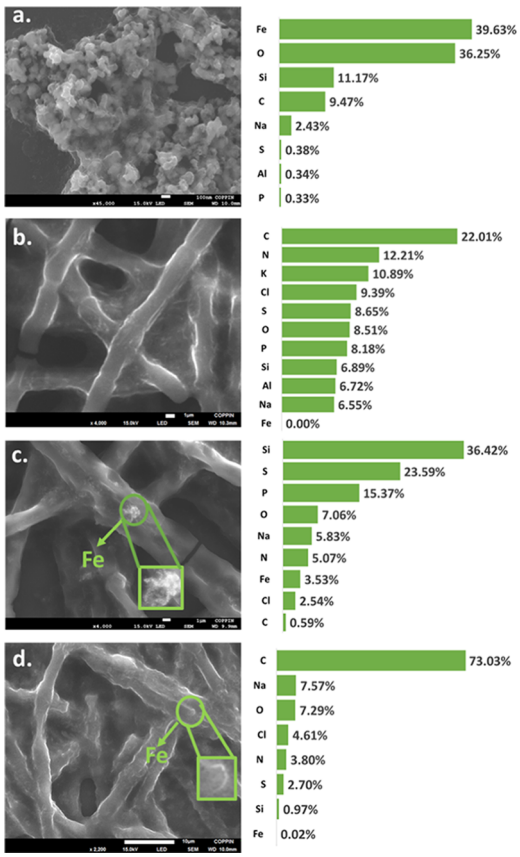


**Figure 6.** FESEM imaging and corresponding EDS elemental quantitative analysis determined by the atomic percentage of each element detected in (a) pure Nanofer 25s zero-valent nanoparticles (nZVIs), (b) *F. diplosiphon* control culture grown in the absence of nZVIs, (c) cultures treated with 3.2 mg $L^{-1}$ nZVIs and (d) 0.8 mg $L^{-1}$ nZVIs.

exposed to 0.8 and 1.6 mg $L^{-1}$ Nanofer 25s (Figure 5) and identified FAME components that were not detected in 1-D GC−MS (i.e., C18:3 and C18:4). The increased proportion of unsaturated FAMES suggests the higher potential of *F. diplosiphon* nanotreated cultures. It is known that nanoparticles improve catalytic efficiency during the transesterifcation process, resulting in high biodiesel production. Excellent magnetic response resulting in high yield of 94% with a biodiesel conversion above 82% after seven cycles was detected using $Fe_3O_4$/ZnMg(Al)O magnetic nanoparticles in biodiesel production.[28]

FESEM validated the aggregation and localization of nZVIs in *F. diplosiphon*. Elemental distribution provided a relative comparison of the nZVIs and the amount of iron detected (Figure 6), considering the fact that nZVIs aggregate differently based on varying nZVI-*F. diplosiphon* attachment. It is not surprising to observe other elements in Nanofer 25s nZVIs as they are known to be coated with organic materials. Our findings are supported by previous characterization of nZVIs using EDS, in which these nanoparticles have been reported to consist of silicon precursors.[29] Considering the small size of nZVIs of 50 nm, it is possible for these nanoparticles to be nonantagonistically up taken into *F. diplosiphon* cells, which are about 6−8 micrometers in cell length.[30] Quantitative charge imaging of individually charged semiconductor nanoparticles on conductive substrates by electric force microscopy and fluorescence tagging will be pursued in future, which will provide insight on nZVI entry into *F. diplosiphon* cells.

## CONCLUSIONS

The results of our study indicate that Nanofer 25s nZVIs at optimal concentrations enhance total lipid content as well as oleic and linoleic acids in *F. diplosiphon*, which are primary fatty acid components in biofuel production. In addition, enhancement of the unsaturated FA profile benefits *F. diplosiphon*-derived biodiesel by reducing the cloud and pour points, thus increasing the percentage of biofuels that could be used in commercial blends. Optimizing scale-up cultivation, harvest, and lipid extraction/conversion to determine the viability of *F. diplosiphon* nanotreated cells for efficient biofuel production is underway.

## EXPERIMENTAL SECTION

**Strains and Culture Conditions.** *F. diplosiphon* strains (SF33 and B481) were grown in 25 vented tissue culture flasks containing BG-11 media, under white light with continuous shaking at 70 rpm and 28 °C. Light intensity was adjusted to 30 $\mu$mol $m^{-2}$ $s^{-1}$ using the model LI-190SA quantum sensor (Li-Cor, Lincoln, NE). Two types of zero-valent iron nanoparticles Nanofer 25 and Nanofer 25s (Nano iron company, Rajhrad, Czech Republic) were tested in this study. Both Nanofers were of an average size of 50 nm, with surface area of 20−25 $m^2$ $g^{-1}$ and a high content of iron;


https://dx.doi.org/10.1021/acsomega.0c00566
ACS Omega XXXX, XXX, XXX−XXX

however, Nanofer 25s contained an extra biodegradable organic surface.

**Impact of Nanofer 25 and 25s on *F. diplosiphon* Growth and Pigmentation.** The impact of Nanofer 25 and Nanofer 25s on *F. diplosiphon* was investigated to determine the effect of nanoparticle-mediated iron stress on cell growth and pigment accumulation. *F. diplosiphon* strains (B481 and SF33) were grown in BG11/HEPES liquid media containing 0.05, 0.1, 0.2, 0.4, 0.8, 1.6, and 3.2 mg $L^{-1}$ Nanofer 25 and Nanofer 25s. Cultures containing Fe−ethylenediaminetetraacetic acid (EDTA) (0.5 mg $L^{-1}$ Fe) served as the control. Three replicates were maintained and cultures were grown for 15 days under constant shaking at 28 °C and 70 rpm, with an initial optical density of 0.1 at 750 nm. To test the impact of nZVIs on photosynthetic efficiency, chlorophyll *a* (chl*a*), carotenoids, and phycobiliprotein levels were quantified as described by De Marsac and Houmard.[31] Phycobiliprotein levels were calculated according to the procedure described by Kahn et al.[32] and reported relative to chl*a*.[33] Significance among cumulative treatment means of growth and pigment levels was determined using ANOVA and Tukey's honest significant difference post-hoc test at 95% confidence intervals ($P < 0.05$). All experiments were repeated once.

**Total Lipid content and Fatty Acid Methyl Esters in *F. diplosiphon* Nanotreated Cells by Gravimetric Analysis, GC−MS, and GC × GC−TOFMS.** We identified total lipid content in *F. diplosiphon* cultures using the chloroform/methanol extraction method based on Folch et al.[34] reported in Wahlen et al.[35] Conversion to FAMEs via direct transesterification was performed as described by Wahlen et al.[35] and modified by Tabatabai et al.[13] In addition, we determined FAME compositions of *F. diplosiphon* transesterified lipids using a Shimadzu GC17A/QP5050A GC−MS combination (Shimadzu Instruments) at the mass spectrometry facility at the Johns Hopkins University (Baltimore, MD). The GC17A was equipped with a low-polarity (5% phenyl-, 95% methylsiloxane) capillary column (30 m length, 0.25 mm ID, 0.25 μm film thickness, and 10 m length guard column). Peaks were identified by comparing mass spectra to the lipid Web Archive of FAME mass spectra. To identify additional FAMEs from the *F. diplosiphon* nanotreated cells and control, we used high-resolution two-dimensional gas chromatography with time-of-flight mass spectrometry (GC × GC−TOFMS) from LECO. We extracted total lipids and subjected to direct transesterification as explained above. The first dimension column was a BP-1 (60 mm × 0.25 mm ID, 0.25 μm film thickness, 100% polysiloxane, SGE Inc.) and the second was a BPX50 (1.5 mm × 0.1 mm ID, 0.1 μm film thickness, 50% phenyl, SGE, Inc.). The GC oven temperature was initially held at 40 °C for 0.5 min, then ramped at 2 °C $min^{-1}$ to 340 °C, and held at a final temperature for 10 min. The secondary oven had a temperature offset of +5 °C from the first oven. The modulator had an offset of +10 °C with a modulation period of 6 s and hot pulse of 0.8 s. Mass spectrometry data were collected with an acquisition rate of 100 spectra/s and mass range from $m/z$ 40 to 550. For all experiments, three biological replicates were maintained and the experiment repeated once. The chemical and physical properties of the transesterified lipids from FAMEs (wt %) in control and nanotreated cells were calculated using BiodieselAnalyzer software version 2.2.[36]

**Field-Emission Scanning Electron Microscopy (FESEM) and Energy-Dispersive X-ray Spectroscopy (EDS).** We visualized the morphology of nZVIs using field-emission scanning electron microscopy (JSM 7100F, JEOL.-COM). Elemental analysis of the samples was investigated at day 12 using Dispersive X-ray Analyzer (EX-37001, Tokyo, Japan) equipped with JED-2300 Series Standard software, at a magnification of 2000 to 4000×. Samples for the EDS measurements were prepared on silicon wafers on a homogeneous and flat surface. Multiple measurements were performed at different areas of the sample and the average computed.

**Statistical Analysis.** Growth, photosynthetic pigment accumulation, total lipid content, and FAME results were reported as a cumulative treatment mean ± standard error. Statistical significance was determined using one-way analysis of variance and Tukey's Honest Significant Difference post-hoc test at 95% confidence intervals ($P < 0.05$).

## ■ ASSOCIATED CONTENT

### Supporting Information

The Supporting Information is available free of charge at https://pubs.acs.org/doi/10.1021/acsomega.0c00566.

*F. diplosiphon* growth in medium containing varying Nanofer 25 nanoparticle concentrations; impact of Nanofer 25s on *F. diplosiphon* pigment accumulation (PDF)

## ■ AUTHOR INFORMATION


### Corresponding Author

**Viji Sitther** − *Department of Biology, Morgan State University, Baltimore, Maryland 21251, United States;* orcid.org/0000-0003-0096-569X

### Authors

**Somayeh Gharaie Fathabad** − *Department of Biology, Morgan State University, Baltimore, Maryland 21251, United States*

**Behnam Tabatabai** − *Department of Biology, Morgan State University, Baltimore, Maryland 21251, United States*

**Dy'mon Walker** − *Department of Biology, Morgan State University, Baltimore, Maryland 21251, United States*

**Huan Chen** − *National High Magnetic Field Laboratory, Florida State University, Tallahassee, Florida 32310, United States*

**Jie Lu** − *National High Magnetic Field Laboratory and Future Fuels Institute, Florida State University, Tallahassee, Florida 32310, United States*

**Kadir Aslan** − *Department of Chemical Engineering, Morgan State University, Baltimore, Maryland 21251, United States;* orcid.org/0000-0002-7617-0175

**Jamal Uddin** − *Center for Nanotechnology, Department of Natural Sciences, Coppin State University, Baltimore, Maryland 21216, United States*

**William Ghann** − *Center for Nanotechnology, Department of Natural Sciences, Coppin State University, Baltimore, Maryland 21216, United States*

Complete contact information is available at: https://pubs.acs.org/10.1021/acsomega.0c00566


### Notes

The authors declare no competing financial interest.

## ■ ACKNOWLEDGMENTS

This study was supported by the National Science Foundation's Division of Engineering [CBET-1900966] and

National Institutes of Health [UL1GM118973] grants awarded to Morgan State University. Work performed at the National High Magnetic Field Laboratory was supported by the National Science Foundation Division of Chemistry [DMR-1644779] and the State of Florida.

## REFERENCES

(1) Grzesik, M.; Romanowska-Duda, Z.; Kalaji, H. M. Effectiveness of cyanobacteria and green algae in enhancing the photosynthetic performance and growth of willow (*Salix viminalis* L.) plants under limited synthetic fertilizers application. *Photosynthetica* **2017**, *55*, 510−521.

(2) Nozzi, N. E.; Oliver, J. W. K.; Atsumi, S. Cyanobacteria as a platform for biofuel production. *Front. Bioeng. Biotechnol.* **2013**, *1*, 7.

(3) Quintana, N.; Van der Kooy, F.; Van de Rhee, M. D.; Voshol, G. P.; Verpoorte, R. Renewable energy from Cyanobacteria: energy production optimization by metabolic pathway engineering. *Appl. Microbiol. Biotechnol.* **2011**, *91*, 471−490.

(4) Sekoai, P. T.; Ouma, C. N. M.; du Preez, S. P.; Modisha, P.; Engelbrecht, N.; Bessarabov, D. G.; Ghimire, A. Application of nanoparticles in biofuels: an overview. *Fuel* **2019**, *237*, 380−397.

(5) Tabatabai, B.; Fathabad, S. G.; Bonyi, E.; Rajini, S.; Aslan, K.; Sitther, V. Nanoparticle mediated impact on growth, photosynthetic efficacy, and fatty acid methyl ester composition in the cyanobacterium *Fremyella diplosiphon*. *BioEnerg. Res.* **2019**, *12*, 409−418.

(6) Nath, D.; Manhar, A. K.; Gupta, K.; Saikia, D.; Das, S. K.; Mandal, M. Photosynthesized iron nanoparticles: effects on fermentative hydrogen production by *Enterobacter cloacae* DH-89. *Bull. Mater. Sci.* **2015**, *38*, 1533−1538.

(7) Kadar, E.; Rooks, P.; Lakey, C.; White, D. A. The effect of engineered iron nanoparticles on growth and metabolic status of marine microalgae cultures. *Sci. Total Environ.* **2012**, *439*, 8−17.

(8) Pádrová, K.; Lukavský, J.; Nedbalová, L.; Čejková, A.; Cajthaml, T.; Sigler, K.; Vítová, M.; Řezanka, T. Trace concentrations of iron nanoparticles cause overproduction of biomass and lipids during cultivation of cyanobacteria and microalgae. *J. Appl. Phycol.* **2015**, *27*, 1443−1451.

(9) Su, L.; Shi, X.; Guo, G.; Zhao, A.; Zhao, Y. Stabilization of sewage sludge in the presence of nanoscale zero-valent iron (nZVI): abatement of odor and improvement of biogas production. *J. Mater. Cycles Waste Manage.* **2013**, *15*, 461−468.

(10) Yan, W.; Herzing, A. A.; Kiely, C. J.; Zhang, W.-X. Nanoscale zero-valent iron (nZVI): aspects of the core-shell structure and reactions with inorganic species in water. *J. Contam. Hydrol.* **2010**, *118*, 96−104.

(11) Gutu, A.; Alvey, R. M.; Bashour, S.; Zingg, D.; Kehoe, D. M. Sulfate-driven elemental sparing is regulated at the transcriptional and posttranscriptional levels in a filamentous cyanobacterium. *J. Bacteriol.* **2011**, *193*, 1449−1460.

(12) Pattanaik, B.; Busch, A. W. U.; Hu, P.; Chen, J.; Montgomery, B. L. Responses to iron limitation are impacted by light quality and regulated by RcaE in the chromatically acclimating cyanobacterium *Fremyella diplosiphon*. *Microbiology* **2014**, *160*, 992−1005.

(13) Tabatabai, B.; Chen, H.; Lu, J.; Giwa-Otusajo, J.; McKenna, A. M.; Shrivastava, A. K.; Sitther, V. *Fremyella diplosiphon* as a biodiesel agent: Identification of fatty acid methyl esters via microwave-assisted direct in situ transesterification. *BioEnerg. Res.* **2018**, *11*, 528−537.

(14) Pattanaik, B.; Montgomery, B. L. A novel role for a TonB-family protein and photo regulation of iron acclimation in *Fremyella diplosiphon*. *Plant Signaling Behav.* **2010**, *5*, 851−853.

(15) Liu, X.; Saydah, B.; Eranki, P.; Colosi, L. M.; Mitchell, B. G.; Rhodes, J.; Clarens, A. F. Pilot-scale data provide enhanced estimates of the life cycle energy and emissions profile of algae biofuels produced via hydrothermal liquefaction. *Bioresour. Technol.* **2013**, *148*, 163−171.

(16) Zhu, L. D.; Li, Z. H.; Hiltunen, E. Strategies for lipid production improvement in microalgae as a biodiesel feedstock. *BioMed Res. Int.* **2016**, *2016*, No. 8792548.

(17) Eglal, M. M.; Ramamurthy, A. S. Nanofer zvi: morphology, particle characteristics, kinetics, and applications. *J. Nanomater.* **2014**, *2014*, No. 152824.

(18) Kirschling, T. L.; Gregory, K. B.; Minkley, E. G., Jr.; Lowry, G. V.; Tilton, R. D. Impact of nanoscale zero valent iron on geochemistry and microbial populations in trichloroethylene contaminated aquifer materials. *Environ. Sci. Technol.* **2010**, *44*, 3474−3480.

(19) Akbarnezhad, M.; Mehrgan, M. S.; Kamali, A.; Baboli, M. J. Bioaccumulation of $Fe^{+2}$ and its effects on growth and pigment content of spirulina (*Arthrospira platensis*). *AACL Bioflux* **2016**, *9*, 227−238.

(20) Ko, K.-S.; Koh, D.-C.; Kong, I. Toxicity evaluation of individual and mixtures of nanoparticles based on algal chlorophyll content and cell count. *Materials* **2018**, *11*, No. 121.

(21) Ševců, A.; El-Temsah, Y. S.; Joner, E. J.; Černík, M. Oxidative stress induced in microorganisms by zero-valent iron nanoparticles. *Microbes Environ.* **2011**, *26*, 271−281.

(22) Kang, N. K.; Lee, B.; Choi, G.-G.; Moon, M.; Park, M. S.; Lim, J.; Yang, J. W. Enhancing lipid productivity of *Chlorella vulgaris* using oxidative stress by $TiO_2$ nanoparticles. *Korean J. Chem. Eng.* **2014**, *31*, 861−867.

(23) Chisti, Y. Biodiesel from microalgae. *Biotechnol. Adv.* **2007**, *25*, 294−306.

(24) Knothe, G. Dependence of biodiesel fuel properties on the structure of fatty acid alkyl esters. *Fuel Process. Technol.* **2005**, *86*, 1059−1070.

(25) Adarme-Vega, T. C.; Thomas-Hall, S. R.; Schenk, P. M. Towards sustainable sources for omega-3 fatty acids production. *Curr. Opin. Biotechnol.* **2014**, *26*, 14−18.

(26) Huang, X.; Wei, L.; Huang, Z.; Yan, J. Effect of high ferric ion concentrations on total lipids and lipid characteristics of *Tetraselmis subcordiformis*, *Nannochloropsis oculata* and *Pavlova viridis*. *J. Appl. Phycol.* **2014**, *26*, 105−114.

(27) Latifi, A.; Jeanjean, R.; Lemeille, S.; Havaux, M.; Zhang, C.-C. Iron starvation leads to oxidative stress in *Anabaena* sp. strain PCC 7120. *J. Bacteriol.* **2005**, *187*, 6596−6598.

(28) Chen, Y.; Liu, T.; He, H.; Liang, H. Fe3O4/ZnMg(Al)O magnetic nanoparticles for efficient biodiesel production. *Appl. Organomet. Chem.* **2018**, *32*, No. e4330.

(29) Stoeva, S. I.; Huo, F.; Lee, J.-S.; Mirkin, C. A. Three-Layer Composite Magnetic Nanoparticle Probes for DNA. *J. Am. Chem. Soc.* **2005**, *127*, 15362−15363.

(30) Bordowitz, J. R.; Montgomery, B. L. Photoregulation of cellular morphology during complementary chromatic adaptation requires sensor-kinase-class protein RcaE in *Fremyella diplosiphon*. *J. Bacteriol.* **2008**, *190*, 4069−4074.

(31) de Marsac, N. T.; Houmard, J. Complementary chromatic adaptation: physiological conditions and action spectra. *Methods Enzymol.* **1988**, *167*, 318−328.

(32) Kahn, K.; Mazel, D.; Houmard, J.; de Marsac, N. T.; Schaefer, M. R. A role for cpeYZ in cyanobacterial phycoerythrin biosynthesis. *J. Bacteriol.* **1997**, *179*, 998−1006.

(33) Whitaker, M. J.; Bordowitz, J. R.; Montgomery, B. L. CpcF-dependent regulation of pigmentation and development in *Fremyella diplosiphon*. *Biochem. Biophys. Res. Commun.* **2009**, *389*, 602−606.

(34) Folch, J.; Lees, M.; Sloane Stanley, G. H. A simple method for the isolation and purification of total lipids from animal tissues. *J. Biol. Chem.* **1957**, *226*, 497−509.

(35) Wahlen, B. D.; Willis, R. M.; Seefeldt, L. C. Biodiesel production by simultaneous extraction and conversion of total lipids from microalgae, cyanobacteria, and wild mixed-cultures. *Bioresour. Technol.* **2011**, *102*, 2724−2730.

(36) Talebi, A. F.; Tabatabaei, M.; Chisti, Y. BiodieselAnalyzer: a user-friendly software for predicting the properties of prospective biodiesel. *Biofuel Res. J.* **2014**, *1*, 55−57.



https://dx.doi.org/10.1021/acsomega.0c00566
ACS Omega XXXX, XXX, XXX−XXX